J Nanopart Res (2011) 13:1723–1735
DOI 10.1007/s11051-010-9927-0

RESEARCH PAPER

Influence of morphology in the catalytic activity of bioconjugated platinum nanostructures

Javier Guerra · Justin L. Burt · Domingo A. Ferrer · Sergio Mejía · Miguel José-Yacamán

Received: 12 October 2009 / Accepted: 8 April 2010 / Published online: 27 April 2010

Abstract Platinum nanoparticles stabilized by a protein, bovine serum albumin, have been synthesized successfully with two different morphologies such as cuboctahedra and nanorods. They have been characterized by the use of different techniques such as XPS, PCS, TEM, and STEM-HAADF. These nanoparticles have been applied as catalysts for the hydrogenation of allyl alcohol in an aqueous solution. A key finding of this article is the superior catalytic activity of the nanorods compared to the cuboctahedral particles. This difference in the catalytic activity was justified because of the variation in the amount of protein to stabilize the nanorods. A model for the nanorods and equations that describe the proportion of atoms in the different sites of the particle (face, vertex, edge, or interior) is used to calculate the percentage of atoms that are located on the nanorod surface. The stability of these particles as catalysts was also studied. The results showed that Pt nanorods and Pt cuboctahedra particles were degraded after 24 h of reaction.

Keywords Nanoparticle · Platinum · BSA · Catalysis · TEM · Protein stabilizing agent

Electronic supplementary material The online version of this article (doi:10.1007/s11051-010-9927-0) contains supplementary material, which is available to authorized users.

J. Guerra
Department of Chemistry and Biochemistry, The University of Texas at Austin, 1 University Station, A5300, Austin, TX 78712-0165, USA

J. Guerra
Departamento de Ciencias Médicas, CIBERNED, Unidad Asociada Neurodeath, CSIC-Universidad de Castilla-La Mancha, 02006 Albacete, Spain

J. L. Burt
Department of Chemical Engineering, The University of Texas at Austin, 1 University Station, MS C0400, Austin, TX 78712-0165, USA

D. A. Ferrer
Microelectronics Research Center, The University of Texas at Austin, 10100 Burnet Road, R9900, Austin, TX 78758-4445, USA

S. Mejía
Facultad de Ciencias Físico-Matemáticas, Universidad Autónoma de Nuevo León, Ciudad Universitaria, San Nicolás de los Garza, NL 66450, Mexico

M. José-Yacamán (✉)
Department of Physics and Astronomy, University of Texas at San Antonio, San Antonio, TX 78249-1644, USA
e-mail: miguel.yacaman@utsa.edu

Introduction

Biologically active molecules have been utilized as ligands for metallic nanoparticles over the last two decades (Mirkin et al. 1996; Schaaff et al. 1998; Templeton et al. 1999) for a wide range of purposes such as sensing, catalysis, or molecular electronics (Choi et al. 2006; Mark et al. 2006; Naik et al. 2004; Niemeyer 2001; Pacardo et al. 2009; Reiss et al. 2004; Yi et al. 2005). However, the control over the nanoparticle size and shape is not yet fully understood (Burda et al. 2005; Jose-Yacaman et al. 2001). Nanoparticles can be embedded in protein structures that will act as cages (Uchida et al. 2007; Varpness et al. 2005) avoiding their aggregation and coalescence.

One of the distinctive characteristics of these nanocomposites is their high surface-to-volume ratio, which makes them ideal for catalysis (Astruc 2007). While it is true that a certain measure of control over catalytic activity can be achieved by regulating the size of platinum nanocrystals (Rioux et al. 2005; Song et al. 2006; Ye et al. 2007), a greater degree of control can be achieved when crystal morphology is also well-regulated (Lee et al. 2006; Rioux et al. 2006). In terms of shape control, Tian et al. have reported tetrahexahedral (THH) platinum particles that display a 400% enhancement compared with the activity exhibited by platinum nanospheres for the electro-oxidation of small organic fuels (Tian et al. 2007). Different authors have also contributed toward understanding the correlation between nanoparticle shapes and the catalytic activity (Burda et al. 2005; Finney and Finke 2008; Narayanan and El-Sayed 2004). One of the main key findings is that aggregated material often is more catalytically active than individual particles (Besson et al. 2005a, b; Narayanan and El-Sayed 2003, 2005).

BSA is a globular protein consisting of a single polypeptide chain with 583 amino acid residues, and its ability to form complexes with different noble-metal nanoparticles has been studied previously with silver (Elechiguerra et al. 2005), gold (Burt et al. 2004), platinum (Burt 2007), and others (Bakshi et al. 2009). The interactions between protein and nanoparticles do not poison the whole surface of the metallic entity, as we have shown in the concentration-dependent suppression of the biological activity of virus HIV-1 (Elechiguerra et al. 2005). BSA protein has also been widely used as stabilizing agent for nanomaterials (Bakshi et al. 2009; Bunker et al. 2007; Meziani et al. 2005; Shang et al. 2007). Interestingly, shape-control of platinum nanoparticles using BSA as capping agent has not been reported. The reactivity of BSA-protected Pt nanoparticles with different morphologies for catalytic applications remains as a fundamental issue to be addressed. The overall kinetics of chemical processes could be influenced by the relative abundance of different catalytic sites in the nanoparticle.

In this article, we report the synthesis, characterization, and the catalytic activity of cuboctahedral platinum nanoparticles and platinum nanorods in the hydrogenation of allyl alcohol. Different techniques such as XPS, PCS, TEM, and STEM-HAADF have been used to fully characterize these materials. The use of this catalytic reaction highlights the distinct performance exhibited by the two different platinum nanocrystal morphologies, namely, cuboctahedral particles and nanorods. The amount of BSA protein that acts as stabilizing agent as well as template is critical for the catalytic activity. We also propose a theoretical model for the nanorods that determines the number of atoms on faces, vertices, and edges. Although the model is simplistic because it assumes that all the nanorods are perfect, we believe it will be particularly helpful for future catalytic applications of nanorods because to our knowledge, there is not such as approach like this in the literature. In addition, we explain the stability of these materials throughout the course of the hydrogenation reaction.

Experimental details

Chemicals

Hexachloroplatinic acid hexahydrate ($H_2PtCl_6{\cdot}6H_2O$, ACS reagent grade), sodium borohydride ($NaBH_4$, 99.9%, Reagent Plus), both purchased from Sigma-Aldrich, Inc. (Milwaukee, WI), bovine serum albumin [BSA; Fraction V, heat shock treated; Fisher Scientific (Pittsburgh, PA)] and allyl alcohol (+99%, Acros Organics, Inc., Morris Plains, NJ) were used without further purification. To prepare aqueous solutions, 18 M Ω cm Milli-Q deionized water (Millipore) was employed. Industrial Hydrogen gas (Praxair, 99.9%) was used for the hydrogenation experiments. All the experiments were carried out under air unless otherwise stated in the text.

Nanocrystal synthesis

Protein-functionalized platinum nanocrystals were synthesized in air by reduction in a homogeneous solution at ambient conditions. $H_2PtCl_6 \cdot 6H_2O$ was reduced in water and in the presence of BSA by the addition of $NaBH_4$.

The syntheses of both platinum samples have been reported elsewhere (Burt 2007). Briefly, 2 mL of 0.075 M H_2PtCl_6 (150 μmol Pt) were added to an aqueous solution containing either 6.250 μmol (0.415 g) or 1.562 μmol (0.104 g) dissolved BSA protein for the synthesis of cuboctahedral particles or the synthesis of nanorods, respectively. Then, 2 mL of freshly prepared 0.6 M $NaBH_4$ aqueous solution (1200 μmol $NaBH_4$) was added rapidly under vigorous stirring, bringing the total volume to 40.0 mL. The molar ratio of $[BH_4^-]$:$[PtCl_6^{2-}]$ was (8:1), and the ratio of [Pt]:[BSA] was either (24:1) for cuboctahedral particles or (96:1) for nanorods. The reaction was allowed to proceed under vigorous stirring for 30 min.

Characterization

X-Ray photoelectron spectroscopic (XPS) studies

The experiments were carried out in a Kratos Analytical Axis Ultra DLD instrument with a monochromatic Al Kα (15 keV) anode. The survey spectra were collected with a step size of 1 eV, a dwell time of 100–200 ms, and a pass energy of 160 eV while the high resolution spectra were done with a step size of 0.1 eV, a dwell time of 1000 ms, and pass energy of 20 eV. Charge neutralization was used to minimize charging effects in the binding energy values. The samples were prepared delivering 7 μL of the BSA (10 μM) or BSA:Pt solutions (10 μM in BSA) on the surface of a gold wafer. The samples were allowed to dry under air. Au(4f7/2) signal (84.0 eV) of the wafer was chosen as reference.

Photon correlation spectroscopic (PCS) studies

The hydrodynamic diameter of the particles was determined using a dynamic light scattering (DLS, ZetaPlus, Brookhaven, Holtsville, NY) instrument operating at a 90° scattering angle with a 635 nm, 35 mW diode laser source. 3 mL of BSA or BSA:Pt solutions (10 μM in BSA) were used for these studies. The path length of the cuvette was 1 cm. Each sample was run ten times and each run lasting 2 min at 298 K. The data were fitted using the non-negatively constrained least squares (NNLS) (Morrison et al. 1985) algorithm to solve the experimentally measured autocorrelation function.

Transmission electron microscopy (TEM) studies

TEM experiments were performed using a JEOL 2010F transmission electron microscope equipped with Schottky-type field emission gun, ultra-high resolution pole piece (CS = 0.5 mm), an Energy Dispersive X-ray spectrometer (EDS), and a scanning transmission electron microscope (STEM) unit with high angle annular dark field (HAADF) detector operating at 200 kV. Samples for TEM analysis were prepared by allowing a drop of the aqueous product to evaporate on a carbon-coated copper TEM grid. Particle size was measured at 250 K× magnifications and counting 100 particles of different images using SigmaScan Pro software.

Catalytic testing

The catalytic activity was measured in terms of turnover frequency (TOF), or the number of moles of product per mole of catalyst per unit time, under conditions where the catalyst is saturated by the reactants (Boudart 1995). To discern the rate of reaction, the consumption of hydrogen gas was monitored as described elsewhere (Wilson et al. 2006). Briefly, a 20 mL solution containing the platinum catalyst (48 μM Pt) was introduced in a 100 mL three-neck round bottom flask. The system was purged with hydrogen (~18 L/min) for 10 min under maximum stirring speed (1100 rpm) to evacuate the air. Subsequently, the system was sealed and hydrogen was allowed to equilibrate between the aqueous and gas phases for another 10 min under maximum stirring speed. Finally, 0.6 mL of allyl alcohol (8.8 mmol) was injected via syringe. The hydrogenation reaction immediately started, and the decrease in the pressure of hydrogen was measured electronically. The amount of 1-propanol generated is signaled by the amount of moles of hydrogen consumed.

1D 1H NMR experiments were also used to compare the results of the catalytic reactions with those obtained by the decrease in the pressure of hydrogen. These NMR experiments were carried out using a Varian Unity Inova NMR spectrometer operating at 499.7722 MHz for 1H (11.7 T). The spectrometer was equipped with a gradient amplifier and a four-nucleus 5 mm 1H {15N-31P} PFG High-Field Indirect detection probe.

Results and discussion

Characterization of the nanomaterials

The nanocomposites are stabilized by a protein, BSA. Two different types of nanoparticles with different shapes were studied: cuboctahedral (or "near spherical") nanoparticles where the surface is composed mainly by {1,0,0} and {1,1,1} facets (Benfield 1992; van Hardeveld and Hartog 1969) and nanorods. Syntheses at ambient temperature and pressure of the cuboctahedral nanoparticles as well as the nanorods have been reported elsewhere (Burt 2007). Briefly, a dilute solution containing $H_2PtCl_6{\cdot}6H_2O$ was added to an aqueous solution that contained BSA. Immediately after, a solution of the reducing agent $NaBH_4$ in water was added. Introduction of $NaBH_4$ to the reaction vessel caused rapid protein foaming. After addition of $NaBH_4$, the solution turned dark black in less than 5 s, implying the metal reduction. Each reaction was allowed to proceed under vigorous stirring for 30 min. The pH of the solutions after the introduction of reducing agent was 8, which is important for two reasons. First, a basic final pH indicates that sufficient electrons were liberated during the course of the reaction to facilitate reduction of the Pt(IV) ions, and to neutralize the initially acidic pH of solution. Second, BSA protein can adopt different conformations according to the pH (Burt 2007; Shang et al. 2007). These conformations have been proved to play a critical role in the nanoparticle synthesis (Burt 2007; Shang et al. 2007). Control experiments following the aforementioned procedure in the absence of BSA unequivocally lead to Pt precipitation (Figure S1, ESM). This confirms the role of stabilizer played by the protein.

Cuboctahedral nanoparticles and nanorods were characterized by means of TEM and STEM experiments with HAADF detector (Garcia-Gutierrez et al. 2004; Thomas 2008).

Figure 1 shows representative HAADF images of cuboctahedral particles as well as nanorods with their size distribution histograms. The first sample, with 24:1 Pt:BSA ratio, consists of cuboctahedral platinum nanocomposites with a diameter of 2.220 ± 0.294 nm (see Fig. 1a, b). The population distribution shows a monodisperse material with less than 8% of standard deviation. The second sample is composed of 96:1 Pt:BSA ratio and has an average crystal width of 2.233 ± 0.320 nm (see Fig. 1c, d). The nanocrystals formed under these conditions are more polydisperse as observed in the HAADF images, 70% of which have a ratio length:width less than 2 (close to "cuboctahedral shape") and the remaining have a ratio length:width higher than 2 (nanorods) (Fig. 1d). For clarity of discussion, we will define this second sample as nanorods.

The point of differentiation in the syntheses to obtain cuboctahedral nanoparticles or nanorods lies in the ratio between the protein molecules and platinum atoms. Manipulating the molar ratio of BSA molecules to metal atoms allows us to obtain nanomaterials with diverse shapes and distribution of sizes (Carbo-Argibay et al. 2007). Two different molar ratios were used for these studies: Pt to protein ratio of 24:1 gave rise to cuboctahedral particles and 96:1 rendered nanorods. In the latter case, fewer protein molecules are present to stabilize the initially formed platinum nuclei, and so these primary particles tend to grow into secondary nanostructures via twinning processes. The twinning energy of platinum is among the highest exhibited for FCC metals. Consequently, for a platinum nanocrystal growing via multiple twinning events, the energetically favored condition is for the twinning system to propagate in the direction orthogonal to the twin plane (Tadmor and Bernstein 2004). The formation of polyhedral nanocrystals via multiple twinning systems emanating in different directions is energetically unfavorable in the case of platinum (Elechiguerra et al. 2006).

Figure 2 shows characteristic HRTEM images of the sample composed of (96:1) Pt:BSA, also called nanorods. In this case, image (a) corresponds to an elongated platinum nanoparticle whose aspect ratio is higher than 2 while the nanoparticle in image (b) has an aspect ratio less than 2. Image (c) reflects the sample corresponding to (24:1) Pt:BSA that gives rise

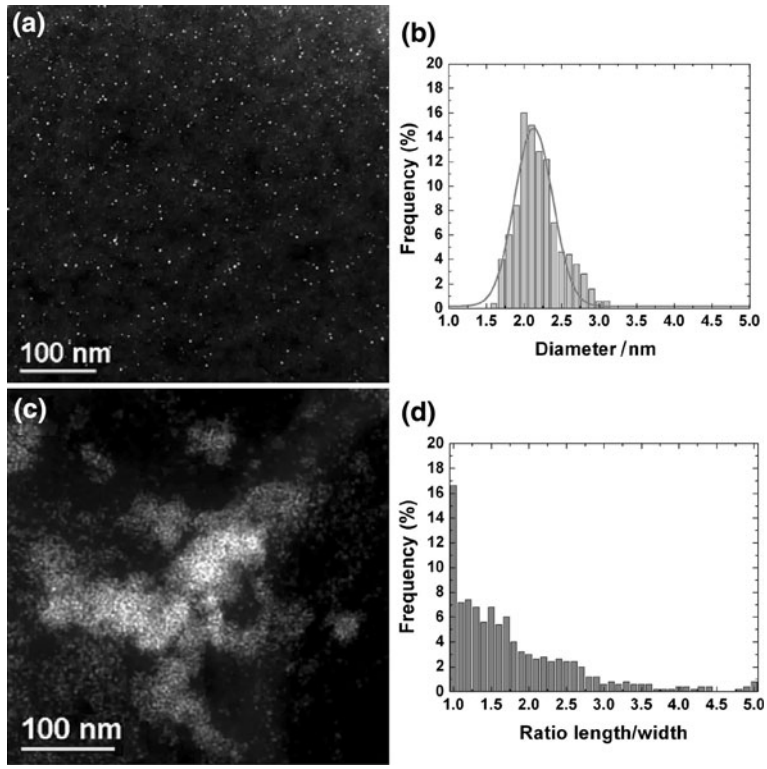

Fig. 1 **a** STEM-HAADF image of cuboctahedral particles, (24:1) Pt:BSA. **b** Size distribution percentage frequency versus diameter in nanometers of the previous image. Diameter = 2.220 ± 0.294 nm. **c** STEM-HAADF image of sample (96:1) Pt:BSA. **d** Product distribution, percentage frequency versus aspect ratio (length:width). Size distribution (length:width) = 1.830 ± 0.857

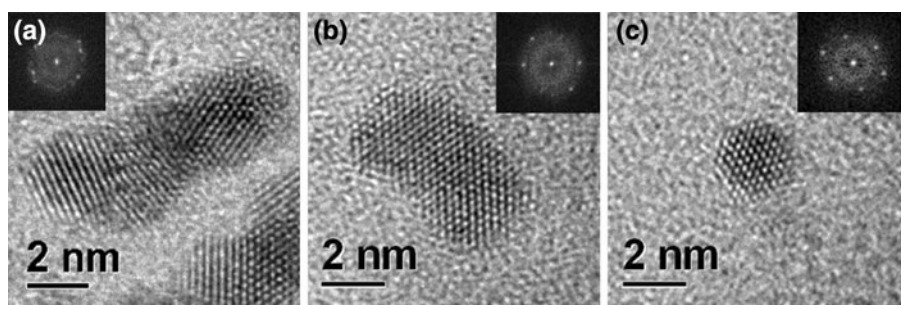

Fig. 2 HRTEM images. **a**, **b** Images corresponding to nanorods, (96:1) Pt:BSA. **c** Image corresponding to a cuboctahedral particle, (24:1) Pt:BSA

to cuboctahedral particles. The fast Fourier transform (FFT) of the crystals in Fig. 2a demonstrates the characteristic spot splitting that is symptomatic of planar twinning. However, no twinning is visible in Fig. 2b, and the FFT does not exhibit spot splitting. It is known that when twin planes are tilted away from the proper zone axis, they become invisible in the electron beam. The FFT of the crystal in this image does not exhibit spot splitting, but it does exhibit spot streaking, which is indicative of twinning, and it is likely that this crystal has also grown by linear twinning. Nanocrystal growth occurs in the direction orthogonal to the twin plane, resulting in an elongated structure. Growth in the direction parallel to the twin plane is largely restricted, with the average breadth of the nanocrystals in the (96:1) Pt:BSA system being nearly unchanged from the sizes measured for the (24:1) Pt:BSA system. This restricted growth limits

the cross-sectional area of the twin plane, thus limiting its total energy, and in fact this energetic consideration may be driving the preferential elongation. Platinum nanocrystals with aspect ratios greater than 2 are formed by the introduction of multiple linear twinning planes. Image (c) shows a characteristic cuboctahedral shape where the interplanar distances were measured from the FFT of each image, and were consistent with the expected values for FCC platinum. Evaluation of the interplanar distances and angular relations of the lattice planes indicates no deviation from the bulk FCC lattice.

XPS studies

XPS experiments have been performed to study the composition of the protein-functionalized platinum nanoparticles.

Figure 3 shows high-resolution spectra in the platinum region of the complexes result of the interaction between Pt and BSA, before and after reduction for both types of nanoparticles, cuboctahedral particles and nanorods. XPS was used to determine the oxidation state of platinum nanoparticles. Pt(4f) core-levels (7/2 and 5/2) in the BSA:Pt complexes before reduction are shifted to lower binding energies after reduction (Fig. 3). This shift of ~0.7 eV indicates reduction of the platinum atoms. The reduced platinum species display a 1.5 eV shift toward higher binding energies with respect to the bulk Pt (71.2 eV). The presence of charging is not uncommon due to quantum size effects for small

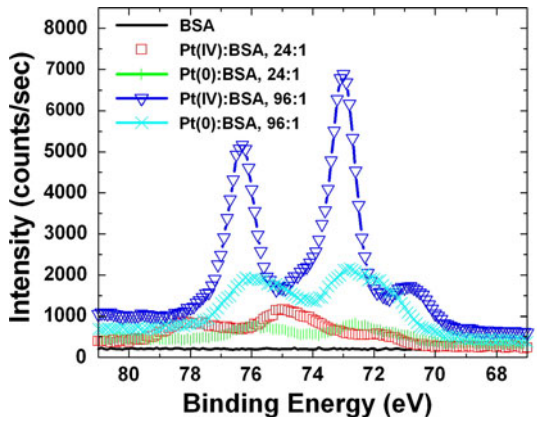

Fig. 3 XPS of pristine BSA, BSA:Pt complexes before and after reduction for cuboctahedral Pt particles and nanorods in the region of Pt 4f5/2 and 4f7/2

platinum (Yang et al. 2006; Ye et al. 2004; Zhao and Crooks 1999) and gold (Hostetler et al. 1998) nanoparticles and has been reported to induce up to a 2 eV displacement (Eberhardt et al. 1990). Therefore, the observed large displacement in energy (1.5 eV) can be attributed to aforementioned effects although an incomplete reduction of the platinum atoms and the presence of PtO, PtO_2, or $Pt(OH)_4$ could be possible. For Pt core-levels (7/2 and 5/2), species such as Pt(0), Pt(II), and Pt(IV) show binding energies of 71.1–74.4, 72.8–76.1, and 74.3–77.6 eV, respectively (Sun et al. 2007; Tian et al. 2006). Incomplete reduction of platinum particles has previously been reported under different conditions (Knecht et al. 2008; Sen and Gokagac 2007). In the XPS survey spectra, the peaks for C(1s), N(1s) and O(1s), S(2p) and Pt(4f) were clearly observed (ESM, Figure S2a–e).

PCS experiments

In order to ascertain the catalytic species in solution, PCS experiments were performed. Dynamic light scattering techniques, such as PCS, are a common tool to study size distributions in situ (Pecora 2000). These studies render the hydrodynamic diameter distribution of the protein–nanoparticle ensemble.

Figure 4 shows PCS experiments performed to study the polydispersity of the cuboctahedral particles and the nanorods in the aqueous solution. The experiments were carried out at a low concentration (10 μM) of BSA to neglect particle–particle interactions and to determine a concentration-independent diffusion coefficient. The hydrodynamic diameter is related to the diffusion coefficient and can be calculated according to the Stokes–Einstein equation (Gomez et al. 2009a, b). Cuboctahedral particles and nanorods exhibited monodispersed size distributions, but in both cases the ascertained sizes were larger than those obtained from TEM measurements. This is due to the fact that the PCS is sensitive to the size of the entire protein–nanoparticle ensemble, while only the metallic crystal lattice is visible under the electron beam in the bright-field TEM techniques (Hayakawa et al. 2003). As expected, PCS studies indicate a smaller size for the protein:Pt cuboctahedron particle ensemble. In fact, the size of pristine BSA under the same basic conditions (~200 eq. of NaBH4, ESM, Figure S3) is very close to the size measured for the cuboctahedral particles. However, it is well known that BSA monomers and

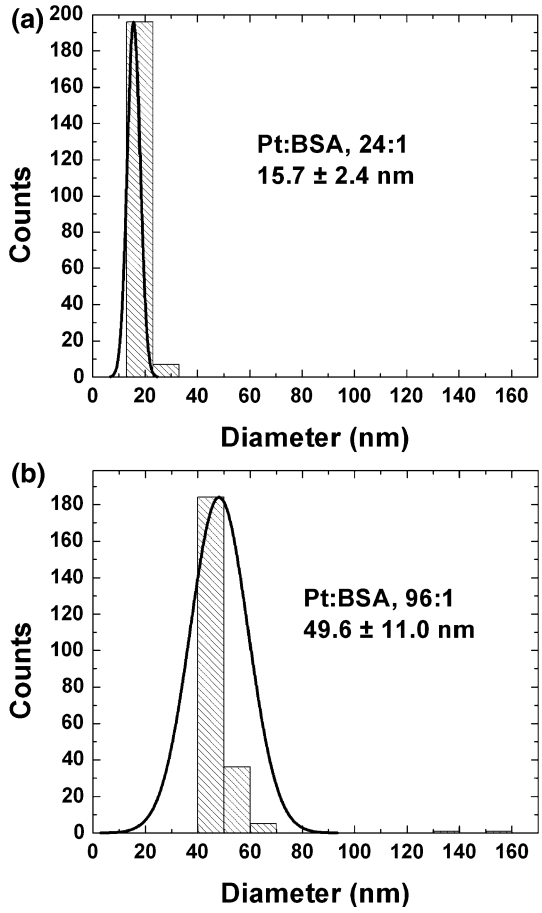

Fig. 4 Size distribution of the BSA:Pt ensemble in solution according to PCS. **a** Cuboctahedral particles, **b** nanorods

dimers have a size estimated to be around 3.7 and 4.8 nm, respectively (Meechai et al. 1999). Our values indicate that the proteins are heavily oligomerized. Serum albumins have a strong tendency to aggregate in solution (Fuentes et al. 2006), and also the use of a strong reducing agent such as $NaBH_4$ can lead to the rupture of the disulfide bonds and the aggregation of these proteins (Sarkar et al. 2007). In any case, BSA under our conditions behaves as a good capping agent, stabilizing the platinum nanoparticles without poisoning their surface. This is essential to obtain a good catalytic activity. In the nanorods, fewer protein molecules are available to stabilize the Pt particles, which results in the formation of bigger aggregates. Such behavior has previously been observed in the synthesis of gold (Pan et al. 2007) and silver (Meziani and Sun 2003) particles using BSA as stabilizer.

Description of the atomic populations located at different sites in the particle

In "structure-sensitive" reactions, every atom in the nanoparticle exhibits a different catalytic activity according to its position and the surrounding environment (Boudart 1995). In the case of cuboctahedral particles, equations reported by Benfield using the mean first-nearest-neighbor coordination number allow us to calculate the number of atoms in different sites (Benfield 1992; van Hardeveld and Hartog 1969). However, no such equations are available for nanorods. In our model, we assume that the nanorod is a result of a varying number of cuboctahedral structures overlapped in one direction. This model was tested by minimizing the energy of diverse structures (ESM, Figure S4). The proposed structures essentially result from the spatial organization of cuboctahedra, which assume a minimum energy by sharing faces. The following equation indicates the number of cuboctahedra that exist in an elongated structure as a function of particle length.

$$N_{CO} = \frac{\sqrt{2}l}{w - r_0}$$

where l is the length, w is the widest axis present in the particle, and r_0 is the distance between the neighboring atoms for the material studied. In the case of a FCC platinum lattice, $r_0 = 0.279$ nm.

Cuboctahedral particle size is determined by the number of shells (υ) around a core atom, where υ is calculated by:

$$\upsilon = \frac{w}{2r_0}$$

Table 1 shows different equations that allow us to estimate the proportion of atoms in every particle according to the site where the atoms are placed (face, edge, vertex, or interior). With the use of the formulae described in the table above, we can assign the location of every atom in the nanorod sample.

The equations (Benfield 1992) and experimentally determined size distribution for the cuboctahedra (Fig. 1b), in combination with the experimental data in Fig. 1d for the nanorods and the equations that describe the number and the location of atoms in these nanoparticles (Table 1), allow us to calculate the proportion of atoms according to the site for both samples (ESM, Figure S5). According to this

Table 1 Equations that describe the number of atoms according to their site in the nanorods surface

Square face atoms	$N_S = (\upsilon - 1)^2(4N_{CO} + 2)$
Triangular face atoms	$N_t = 4(\upsilon - 2)(\upsilon - 1) + [4(\upsilon - 3)(\upsilon - 2) + 4\upsilon - 8](N_{CO} - 1)$
Vertex atoms	$N_\upsilon = 4N_{CO} + 8$
Edge atoms	$N_e = 40(\upsilon - 1) + 16(N_{CO} - 1)(\upsilon - 2)$

figure, nanorods present a higher proportion of atoms in the interior (58%) with respect to cuboctahedral particles (48%). This fact implies that the surface area for the nanorods is less than the one in the cuboctahedral sample. Atoms located in faces (addition of triangular and square faces) represent a 25% for cuboctahedra while the nanorods contain 22.5% of these atoms. A similar trend is observed for defect atoms (addition of vertex and edge atoms) where the proportion of these for the cuboctahedra (27%) is greater than for the nanorods (20%). The ratio of face/defect atoms is close to 1 for both samples. All these data and calculations serve to conclude that both samples have similar atomic distributions, although in a different morphology. From these calculations, and because both samples display analogous atomic distributions, a priori similar catalytic activity should be expected.

Catalytic experiments

To discriminate between the catalytic activity of the cuboctahedral particles and the nanorods, our study targeted the hydrogenation of allyl alcohol. This reaction is structure-sensitive according to a previous study (Wilson et al. 2006). The reaction takes place in aqueous solution and follows the "Horiuti-Polanyi" or "half-hydrogenated" mechanism (Smith and Notheisz 1999). The dissociative adsorption of molecular hydrogen (homolytic rupture of the H–H σ-bond) onto the metallic surface renders two hydrogen atoms. Besides, olefin molecules (allyl alcohol in this study) interact with the metal atoms located on the particle surface. One of these hydrogen atoms attaches to one of the two olefinic sp^2 carbons, providing the half-hydrogenated state. All steps in the process are in equilibrium, and hence are reversible. Once the alkane (1-propanol in this study) is irreversibly formed by addition of a second hydrogen atom, the newly generated molecule desorbs from the surface (Smith and Notheisz 1999).

Mass-transfer limitations in a heterogeneous system should always be taken into account to study different catalytic processes (Aiken III and Finke 1998; Smith and Notheisz 1999). For our particular heterogeneous system, three different phases coexist (hydrogen gas phase, aqueous solution, and nanoparticle surface), and diffusion barriers can interfere with the measured level of catalytic activity. Diverse equations and experiments are reported in the literature to describe how the mass transfer is involved in the determination of the reaction rate (ESM, Figure S6) (Aiken III and Finke 1998; Alcorn and Sullivan 1992; Smith and Notheisz 1999). We have used two sets of experiments to find the conditions for our system where mass transfer limitations are minimized.

Figure 5 shows how to find the appropriate conditions to minimize the mass transfer. In the first set of experiments, different concentrations of cuboctahedral catalyst were tested in the hydrogenation of allyl alcohol. The aim was to determine the region where the catalytic activity (in terms of TOF) is proportional to the concentration of catalyst. In this region, the mass-transfer processes do not have a substantial influence on the catalytic value. Under these conditions, the catalyst is saturated by the reactants and the rate depends on a pseudo-first order rate constant and the catalyst concentration. When the rate is independent of the latter, a plateau can be observed and in this region the reaction is controlled by mass transfer (Fig. 5a). The experimentally obtained concentration of 48 μM of the platinum catalyst implies that at this concentration, the system falls in the intrinsic kinetic regime (Fig. 5 and ESM, Figures S6, S7).

The second set of experiments consists of the measurement of TOFs with different stirring rates. Since the degree of mixing of the reactants depends upon the stirring rate, this may influence the reaction rate. If small changes in the stirring rate do not change the reaction rate, then it implies that the mass transfer process between the gas and liquid phases does not control the overall reaction. We evaluated the stirring-rate dependence for cuboctahedral platinum particles with concentration of 48 μM (Fig. 5b). According to our concentration-dependence set of experiments, this concentration is located in the kinetic regime. The reaction rate was observed to

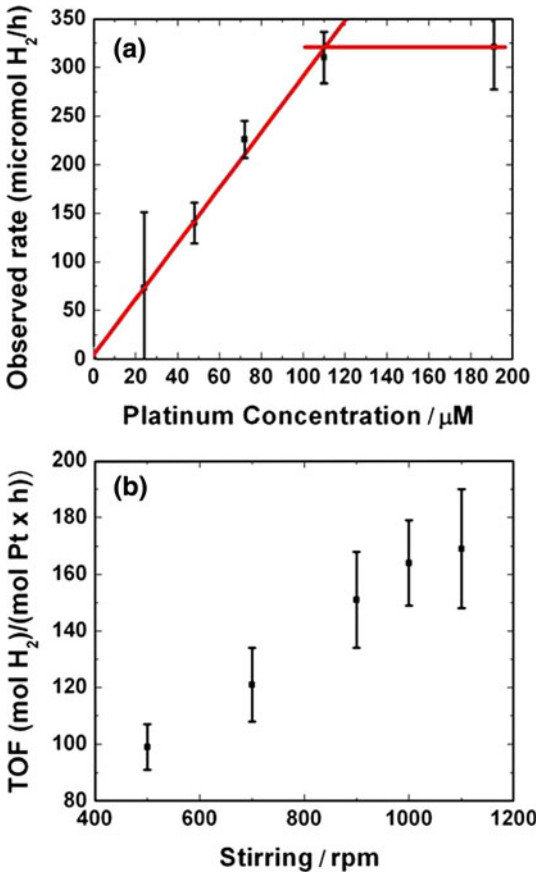

Fig. 5 **a** Rate versus catalyst concentration for (24:1) Pt:BSA nanoparticles. **b** Rate versus stirring rate for 48 μM (24:1) Pt:BSA nanoparticles

level off at high stirring rates. This behavior agrees closely with an intrinsic kinetic regime.

The stirring-rate dependence study was also done for platinum nanorods (48 μM). A plateau in the catalytic activity for high stirring rates was observed (ESM, Figure S8). This experiment confirms that nanorods at a concentration of 48 μM are also in a kinetic regime. If the same experiment is performed with a concentration of 110 μM using cuboctahedral particles, no plateau is reached, which agrees with a process governed by mass-transfer limitations as expected (ESM, Figure S9).

The reactions were run under a known hydrogen pressure. The decrease in the pressure measured during a known period of time allowed us to calculate the amount of hydrogen moles consumed in the reaction and the TOF. The validity of this TOF value was also checked by 1H-NMR (7 h were needed for these experiments). In the 1H-NMR, allyl alcohol and 1-propanol were the chemicals detected, which indicates a high selectivity. It also points toward platinum being a poor catalyst for oxidative dehydrogenation because of the absence of propanaldehyde or propenal (Kereszzegi et al. 2001). 1H-NMR integrals gave us number of moles of 1-propanol that agrees with the decrease in the hydrogen pressure, thus confirming the reliability of calculated TOFs.

To determine TOF values for Pt cuboctahedra particles and nanorods, we have assumed that the whole amount of Pt atoms has been reduced. This assumption is based on the reducing conditions (hydrogen atmosphere) used for our experiments combined with the presence of Pt(0) atoms that could act as catalytic seed for unreduced Pt particles. Cuboctahedral nanoparticles and nanorods were studied as catalysts. TOFs for cuboctahedral particles [169 ± 21 mol H2/(mol Pt × h)] and nanorods [243 ± 29 mol H2/(mol Pt × h)] showed a different catalytic activity. The data revealed that nanorods display the highest catalytic activity in spite of the fact that cuboctahedra particles and nanorods share a similar atomic distribution. We can conclude that nanorods are better catalysts than the cuboctahedra in agreement with previous articles (Besson et al. 2005a, b; Narayanan and El-Sayed 2003; Ott et al. 2007).

It is also worth to mention that nanorods have less Pt atoms on the particle surface (42%) compared with the cuboctahedra (52%) (ESM, Figure S5). The superior catalytic activity of nanorods can be explained on the basis of differences in the amount of protein in both materials. Cuboctahedral particles, monodispersed with a well-defined shape, contain four times the quantity of protein that is present in the nanorods. A higher amount of proteins also implies an increase in the amount of sulfur groups in the solution that can chelate the particle and a more effective stabilization and passivation as the PCS studies suggest. In the nanorods, with a cleaner metallic surface available to perform the reaction and a less effective particle protection, the catalytic activity is better. The catalytic activity measured for both types of BSA-functionalized nanocrystals was greater than the activity reported for dendrimer-encapsulated platinum nanocrystals [TOF = 50 mol H2/(mol Pt × h)] (Scott et al. 2003).

Stability

Platinum particles studied in this work remain stable for months. Nevertheless, when the hydrogenation reaction is performed, a precipitate is observed within 24 h.

In order to study the stability of these bioconjugated protein platinum nanoparticles, hydrogenation reactions were performed and aliquots were taken after 3 and 24 h (ESM, Figures S10, S11). Coalescence of the nanocomposites was observed according to TEM analyses. After 24 h, protein aggregation is clearly visible for the cuboctahedral nanoparticles as well as the nanorods. The precipitate is clearly more noticeable when the cuboctahedral particles are the catalyst, although in this case, BSA protein concentration is also higher (24 platinum atoms per BSA molecule).

Different control experiments were performed to discern the origin of the precipitation. A 20 mL aqueous solution of allyl alcohol (0.6 mL) and 48 μM cuboctahedral platinum particles were stirred at room temperature in the absence of hydrogen. No precipitate was observed after 24 h. A second experiment was carried out stirring a solution of 48 μM cuboctahedral platinum nanoparticles under hydrogen atmosphere. The solution does not change after 24 h and no decrease in the hydrogen pressure was noticed. After this period of time, allyl alcohol was introduced in the system. The hydrogenation reaction took place and after 1 day, a clearly observable precipitate appeared in the system. This experiment was also conducted using platinum nanorods and the same results were obtained. A degradation of the protein is likely to be the cause for this precipitation. The BSA protein has unsaturated residues that are close to the nanoparticle surface and can be reduced. Degradation of unsaturated residues could induce a change in the tertiary structure of the protein, ultimately leading to aggregation of the BSA molecules which is visible at the macroscopic scale, and coalescence among the nanocrystals which is evident at the microscopic scale.

Conclusions

In summary, we have demonstrated that platinum nanocrystals directly conjugated to BSA protein molecules are active toward the catalytic hydrogenation of allyl alcohol. The characterization of the catalysts was performed by means of TEM, XPS, and PCS studies. These experiments suggest that the cuboctahedral nanoparticles are small, well-defined, and monodisperse Pt(0) particles while the nanorods are a polydisperse sample that forms larger aggregates in solution with the BSA. We report the catalytic performance of our materials, with nanorods exhibiting superior activity. We attribute this difference in catalytic activity to the amount of protein used as template in each case. A lesser amount of protein means a cleaner metallic surface available to perform the reaction although the polydispersity of the Pt nanoparticles is higher. A model for the nanorods and equations that describe the proportion of atoms in the different sites of the particle (face, vertex, edge, or interior) is reported. However, the long-term dimensional stability of protein-functionalized platinum nanocrystals was compromised under the catalytic reaction conditions, as documented by TEM analysis. Significant coalescence was observed in the cuboctahedral particles and nanorods after 24 h of reaction within the intrinsic kinetic regime. We attribute the observed protein aggregation and nanocrystal coalescence to the structural degradation of BSA molecules when exposed to the hydrogenation reaction conditions for prolonged time.

Acknowledgments One of us (M.J.Y.) would like to acknowledge support from the Welch Foundation and from the Metals program of the Materials Division of NSF. We are indebted to Prof. Richard M. Crooks for helpful discussion and advice regarding the catalytic experiments and interpretation of the data. We also thank Dr. Ji-Ping Zhou of the Texas Materials Institute at UT-Austin for help with the TEM Measurements as well as V. Sue Myers (Richard M. Crooks' Group) and Dr. Yangming Sun of Center For Nanomolecular Science and Technology at UT-Austin for providing the XPS measurements. J.G. thanks Prof. Gerard V. Smith (Southern Illinois University) for a copy of reference Alcorn and Sullivan 1992. J.G. is indebted to the Junta de Comunidades de Castilla-La Mancha (Spain) for a postdoctoral grant. J.L.B. thanks The University of Texas at Austin College of Engineering for support through the Thrust 2000 Robert L. and Jane G. Mitchell Endowed Graduate Fellowship in Engineering, and the George J. Heuer, Jr. Ph.D. Endowed Graduate Fellowship. This material is based upon work supported under a National Science Foundation Graduate Research Fellowship (to J.L.B.).

References

Aiken JD III, Finke RG (1998) Nanocluster formation synthetic, kinetic, and mechanistic studies. The detection of, and then methods to avoid, hydrogen mass-transfer limitations in the synthesis of polyoxoanion- and tetrabutylammonium-stabilized, near-monodisperse 40 ± 6 Å

Rh(0) nanoclusters. J Am Chem Soc 120(37):9545–9554. doi:10.1021/ja9719485

Alcorn WR, Sullivan TJ (1992) Evaluation of hydrogen catalysts in batch reactors. Chem Catal News, Engelhard Corporation, August 1992

Astruc D (2007) Palladium nanoparticles as efficient green homogeneous and heterogeneous carbon-carbon coupling precatalysts: a unifying view. Inorg Chem 46(6):1884–1894. doi:10.1021/ic062183h

Bakshi MS, Thakur P, Kaur G, Kaur H, Banipal TS, Possmayer F, Petersen NO (2009) Stabilization of PbS nanocrystals by bovine serum albumin in its native and denatured states. Adv Funct Mater 19(9):1451–1458. doi:10.1002/adfm.200801

Benfield RE (1992) Mean coordination numbers and the non-metal-metal transition in clusters. J Chem Soc Faraday Trans 88:1107–1110. doi:10.1039/FT9928801107

Besson C, Finney EE, Finke RG (2005a) Nanocluster nucleation, growth, and then agglomeration kinetic and mechanistic studies: a more general, four-step mechanism involving double autocatalysis. Chem Mater 17(20):4925–4938. doi:10.1021/cm050207x

Besson C, Finney EE, Finke RG (2005b) A mechanism for transition-metal nanoparticle self-assembly. J Am Chem Soc 127(22):8179–8184. doi:10.1021/ja0504439

Boudart M (1995) Turnover rates in heterogeneous catalysis. Chem Rev 95(3):661–666. doi:10.1021/cr00035a009

Bunker CE, Novak KC, Guliants EA, Harruff BA, Meziani MJ, Lin Y, Sun Y-P (2007) Formation of protein-metal oxide nanostructures by the sonochemical method: observation of nanofibers and nanoneedles. Langmuir 23(20):10342–10347. doi:10.1021/la7013682

Burda C, Chen X, Narayanan R, El-Sayed MA (2005) Chemistry and properties of nanocrystals of different shapes. Chem Rev 105(4):1025–1102. doi:10.1021/cr030063a

Burt JL (2007) Formation of noble metal nanocrystals in the presence of biomolecules. PhD Thesis. University of Texas at Austin

Burt JL, Gutierrez-Wing C, Miki-Yoshida M, Jose-Yacaman M (2004) Noble-metal nanoparticles directly conjugated to globular proteins. Langmuir 20(26):11778–11783. doi:10.1021/la048287r

Carbo-Argibay E, Rodriguez-Gonzalez B, Pacifico J, Pastoriza-Santos I, Perez-Juste J, Liz-Marzan LM (2007) Chemical sharpening of gold nanorods: the rod-to-octahedron transition. Angew Chem Int Ed 119(47):8983–8987. doi:10.1002/ange.200703259

Choi J, Jun Y, Yeon S-I, Kim HC, Shin J-S, Cheon J (2006) Biocompatible heterostructured nanoparticles for multimodal biological detection. J Am Chem Soc 128(50):15982–15983. doi:10.1021/ja066547g

Eberhardt W, Fayet P, Cox DM, Fu Z, Kaldor A, Sherwood R, Sondericker D (1990) Photoemission from mass-selected monodispersed Pt clusters. Phys Rev Lett 64(7):780–783. doi:10.1103/PhysRevLett.64.780

Elechiguerra JL, Burt JL, Morones JR, Camacho-Bragado A, Gao X, Lara HH, Jose-Yacaman M (2005) Interaction of silver nanoparticles with HIV-1. J Nanobiotechnol 3(6):1–10. doi:10.1186/1477-3155-3-6

Elechiguerra JL, Reyes-Gasga J, Jose-Yacaman M (2006) The role of twinning in shape evolution of anisotropic noble metal nanostructures. J Mater Chem 16:3906–3919. doi:10.1039/b607128g

Finney EE, Finke RG (2008) Nanocluster nucleation and growth kinetic and mechanistic studies: a review emphasizing transition-metal nanoclusters. J Colloid Interface Sci 317(2):351–374. doi:10.1016/j.jcis.2007.05.092

Fuentes M, Pessela BCC, Mateo C, Palomo JM, Batalla P, Fernández-Lafuente R, Guisán JM (2006) Adsorption behavior of bovine serum albumin on lowly activated anionic exchangers suggests a new strategy for solid-phase proteomics. Biomacromolecules 7(4):1357–1361. doi:10.1021/bm060002x

Garcia-Gutierrez D, Gutierrez-Wing C, Miki-Yoshida M, Jose-Yacaman M (2004) HAADF study of Au-Pt core-shell bimetallic nanoparticles. Appl Phys A 79(3):481–487. doi:10.1007/s00339-004-2600-7

Gomez MV, Guerra J, Velders AH, Crooks RM (2009a) NMR characterization of fourth-generation PAMAM dendrimers in the presence and absence of palladium dendrimer-encapsulated nanoparticles. J Am Chem Soc 131(1):341–350. doi:10.1021/ja807488d

Gomez MV, Guerra J, Myers VS, Crooks RM, Velders AH (2009b) Nanoparticle size determination by 1H NMR spectroscopy. J Am Chem Soc ASAP. doi:10.1021/ja9065442

Hayakawa K, Yoshimura T, Esumi K (2003) Preparation of gold-dendrimer nanocomposites by laser irradiation and their catalytic reduction of 4-nitrophenol. Langmuir 19(13):5517–5521. doi:10.1021/la034339l

Hostetler MJ, Wingate JE, Zhong C-J, Harris JE, Vachet RW, Clark MR, Londono JD, Green SJ, Stokes JJ, Wignall GD, Glish GL, Porter MD, Evans ND, Murray RW (1998) Alkanethiolate gold cluster molecules with core diameters from 1.5 to 5.2 nm: core and monolayer properties as a function of core size. Langmuir 14(1):17–30. doi:10.1021/la970588w

Jose-Yacaman M, Ascencio JA, Liu HB, Gardea-Torresdey J (2001) Structure shape and stability of nanometric sized particles. J Vac Sci Technol B 19(4):1091–1103. doi:10.1116/1.1387089

Kereszzegi C, Mallat T, Baiker A (2001) Selective transfer dehydrogenation of aromatic alcohols on supported palladium. New J Chem 25:1163–1167. doi:10.1039/b102463a

Knecht MR, Weir MG, Myers VS, Pyrz WD, Ye H, Petkov V, Buttrey DJ, Frenkel AI, Crooks RM (2008) Synthesis and characterization of Pt dendrimer-encapsulated nanoparticles: effect of the template on nanoparticle formation. Chem Mater 20(16):5218–5228. doi:10.1021/cm8004198

Lee H, Habas SE, Kweskin S, Butcher D, Somorjai GA, Yang P (2006) Morphological control of catalytically active platinum nanocrystals. Angew Chem Int Ed 45(46):7824–7828. doi:10.1002/anie.200603068

Mark SS, Bergkvist M, Yang X, Angert ER, Batt CA (2006) Self-assembly of dendrimer-encapsulated nanoparticle arrays using 2-D microbial S-layer protein biotemplates. Biomacromolecules 7(6):1884–1897. doi:10.1021/bm0603185

Meechai N, Jamieson AM, Blackwell J (1999) Translational diffusion coefficients of bovine serum albumin in aqueous solution at high ionic strength. J Colloid Interface Sci 218(1):167–175. doi:10.1006/jcis.1999.6401

Meziani MJ, Sun Y-P (2003) Protein-conjugated nanoparticles from rapid expansion of supercritical fluid solution into aqueous solution. J Am Chem Soc 125(26):8015–8018. doi:10.1021/ja030104k

Meziani MJ, Pathak P, Harruff BA, Hurezeanu R, Sun Y-P (2005) Direct conjugation of semiconductor nanoparticles with proteins. Langmuir 21(5):2008–2011. doi:10.1021/la0478550

Mirkin CA, Letsinger RL, Mucic RC, Storhoff JJ (1996) A DNA-method for rationally assembling nanoparticles into macroscopic materials. Nature (Lond) 382:607. doi:10.1038/382607a0

Morrison ID, Grabowski EF, Herb CA (1985) Improved techniques for particle size determination by quasi-elastic light scattering. Langmuir 1(4):496–501. doi:10.1021/la00064a016

Naik RR, Jones SE, Murray CJ, McAuliffe JC, Vaia RA, Stone MO (2004) Peptide templates for nanoparticle synthesis derived from polymerase chain reaction-driven phage display. Adv Funct Mater 14(1):25–30. doi:10.1002/adfm.200304501

Narayanan R, El-Sayed MA (2003) Effect of catalytic activity on the metallic nanoparticle size distribution: electron-transfer reaction between Fe(CN)6 and thiosulfate ions catalyzed by PVP-platinum nanoparticles. J Phys Chem B 107(45):12416–12424. doi:10.1021/jp035647v

Narayanan R, El-Sayed MA (2004) Changing catalytic activity during colloidal platinum nanocatalysis due to shape changes: electron-transfer reaction. J Am Chem Soc 126(23):7194–7195. doi:10.1021/ja0486061

Narayanan R, El-Sayed MA (2005) Effect of colloidal nanocatalysis on the metallic nanoparticle shape: the Suzuki reaction. Langmuir 21(5):2027–2033. doi:10.1021/la047600m

Niemeyer CM (2001) Nanoparticles, proteins, and nucleic acids: biotechnology meets materials science. Angew Chem Int Ed 40(22):4128–4158. doi:10.1002/1521-3773(20011119)40:22<4128:AID-ANIE4128>3.0.CO;2-S

Ott LS, Campbell S, Seddon KR, Finke RG (2007) Evidence that imidazolium-based ionic ligands can be metal(0)/nanocluster catalyst poisons in at least the test case of iridium(0)-catalyzed acetone hydrogenation. Inorg Chem 46(24):10335–10344. doi:10.1021/ic700976z

Pacardo DB, Sethi M, Jones SE, Naik RR, Knecht MR (2009) Biomimetic synthesis of Pd nanocatalysts for the stille coupling reaction. ACS Nano 3:1288–1296. doi:10.1021/nn9002709

Pan B, Cui D, Xu P, Li Q, Huang T, He R, Gao F (2007) Study on interaction between gold nanorod and bovine serum albumin. Colloid Surf A 295(1–3):217–222. doi:10.1016/j.colsurfa.2006.09.002

Pecora R (2000) Dynamic light scattering measurement of nanometer particles in liquids. J Nanopart Res 2(2):123–131. doi:10.1023/A:1010067107182

Reiss BD, Mao C, Solis DJ, Ryan KS, Thomson T, Belcher AM (2004) Biological routes to metal alloy ferromagnetic nanostructures. Nano Lett 4(6):1127–1132. doi:10.1021/nl049825n

Rioux RM, Song H, Hoefelmeyer JD, Yang P, Somorjai GA (2005) High-surface-area catalyst design: synthesis, characterization, and reaction studies of platinum nanoparticles in mesoporous SBA-15 silica. J Phys Chem B 109(6):2192–2202. doi:10.1021/jp048867x

Rioux RM, Song H, Grassa M, Habasa S, Niesz K, Hoefelmeyer JD, Yang P, Somorjai GA (2006) Monodisperse platinum nanoparticles of well-defined shape: synthesis, characterization, catalytic properties and future prospects. Top Catal 39:167–174

Sarkar R, Narayanan SS, Palsson L-O, Dias F, Monkman A, Pal SK (2007) Direct conjugation of semiconductor nanocrystals to a globular protein to study protein-folding intermediates. J Phys Chem B 111(42):12294–12298. doi:10.1021/jp075239h

Schaaff TG, Knight G, Shafigullin MN, Borkman RF, Whetten RL (1998) Isolation and selected properties of a 10.4 kDa gold:glutathione cluster compound. J Phys Chem B 102(52):10643–10646. doi:10.1021/jp9830528

Scott RWJ, Datye AK, Crooks RM (2003) Bimetallic palladium-platinum dendrimer-encapsulated catalysts. J Am Chem Soc 125(13):3708–3709. doi:10.1021/ja034176n

Sen F, Gokagac G (2007) Different sized platinum nanoparticles supported on carbon: an XPS study on these methanol oxidation catalysts. J Phys Chem C 111(15):5715–5720. doi:10.1021/jp068381b

Shang L, Wang Y, Jiang J, Dong S (2007) pH-dependent protein conformational changes in albumin:gold nanoparticle bioconjugates: a spectroscopic study. Langmuir 23(5):2714–2721. doi:10.1021/la062064e

Smith GV, Notheisz F (1999) Heterogeneous catalysis in organic chemistry. pp 3–32

Song H, Rioux RM, Hoefelmeyer JD, Komor R, Niesz K, Grass M, Yang P, Somorjai GA (2006) Hydrothermal growth of mesoporous SBA-15 silica in the presence of PVP-stabilized Pt nanoparticles: synthesis, characterization, and catalytic properties. J Am Chem Soc 128(9):3027–3037. doi:10.1021/ja057383r

Sun Y, Zhuang L, Lu J, Hong X, Liu P (2007) Collapse in crystalline structure and decline in catalytic activity of Pt nanoparticles on reducing particle size to 1 nm. J Am Chem Soc 129(50):15465–15467. doi:10.1021/ja076177b

Tadmor EB, Bernstein N (2004) A first-principles measure for the twinnability of FCC metals. J Mech Phys Solids 52(11):2507–2519. doi:10.1016/j.jmps.2004.05.002

Templeton AC, Chen S, Gross SM, Murray RW (1999) Water-soluble, isolable gold clusters protected by tiopronin and coenzyme A monolayers. Langmuir 15(1):66–76. doi:10.1021/la9808420

Thomas JM (2008) A significant structural advance using stem. ChemPhysChem 9(10):1363–1365. doi:10.1002/cphc.200800190

Tian ZQ, Jiang SP, Liang YM, Shen PK (2006) Synthesis and characterization of platinum catalysts on multiwalled carbon nanotubes by intermittent microwave irradiation for fuel cell applications. J Phys Chem B 110(11):5343–5350. doi:10.1021/jp056401o

Tian N, Zhou Z-Y, Sun S-G, Ding Y, Wang ZL (2007) Synthesis of tetrahexahedral platinum nanocrystals with high-index facets and high electro-oxidation activity. Science 316(5825):732–735. doi:10.1126/science.1140484

Uchida M, Klem MT, Allen M, Suci P, Flenniken M, Gillitzer E, Varpness Z, Liepold LO, Young M, Douglas T (2007) Biological containers: protein cages as multifunctional

nanoplatforms. Adv Mater 19(8):1025–1042. doi:10.1002/adma.200601168

van Hardeveld H, Hartog F (1969) Statistics of surface atoms and surface sites on metal crystals. Surf Sci 15(2):189–230. doi:10.1016/0039-6028(69)90148-4

Varpness Z, Peters JW, Young M, Douglas T (2005) Biomimetic synthesis of a H2 catalyst using a protein cage architecture. Nano Lett 5(11):2306–2309. doi:10.1021/nl0517619

Wilson OM, Knecht MR, Garcia-Martinez JC, Crooks RM (2006) Effect of Pd nanoparticle size on the catalytic hydrogenation of allyl alcohol. J Am Chem Soc 128(14):4510–4511. doi:10.1021/ja058217m

Yang D-Q, Zhang G-X, Sacher E, Jose-Yacaman M, Elizondo N (2006) Evidence of the interaction of evaporated Pt nanoparticles with variously treated surfaces of highly oriented pyrolytic graphite. J Phys Chem B 110(16):8348–8356. doi:10.1021/jp060513d

Ye H, Scott RWJ, Crooks RM (2004) Synthesis, characterization, and surface immobilization of platinum and palladium nanoparticles encapsulated within amine-terminated poly(amidoamine) dendrimers. Langmuir 20(7):2915–2920. doi:10.1021/la0361060

Ye H, Crooks JA, Crooks RM (2007) Effect of particle size on the kinetics of the electrocatalytic oxygen reduction reaction catalyzed by Pt dendrimer-encapsulated nanoparticles. Langmuir 23(23):11901–11906. doi:10.1021/la702297m

Yi H, Nisar S, Lee S-Y, Powers MA, Bentley WE, Payne GF, Ghodssi R, Rubloff GW, Harris MT, Culver JN (2005) Patterned assembly of genetically modified viral nanotemplates via nucleic acid hybridization. Nano Lett 5(10):1931–1936. doi:10.1021/nl051254r

Zhao M, Crooks RM (1999) Dendrimer-encapsulated Pt nanoparticles: synthesis, characterization, and applications to catalysis. Adv Mater 11(3):217–220